Supporting Information

For

Room Temperature Wet Chemical Synthesis of Au NPs/TiH_2/nanocarved Ti Self-supported Electrocatalysts for Highly Efficient H_2 Generation

Mohammed A. Amin[1,3]*, Sahar A. Fadlallah[4], Ghaida S. Alosaimi[1], Emad M. Ahmed[2,5], Nasser Y. Mostafa[1,6], Pascal Roussel[7], Sabine Szunerits[8], Rabah Boukherroub[8]

[1]*Materials science and engineering group, Department of Chemistry, Faculty of Science, Taif University, 888 Hawiya, Saudi Arabia*

[2]*Materials science and engineering group, Department of Physics, Faculty of Science, Taif University, 888 Hawiya, Saudi Arabia*

[3]*Department of Chemistry, Faculty of Science, Ain Shams University, 11566 Abbassia, Cairo, Egypt*

[4]*Chemistry Department, Faculty of Science, Cairo University, 12613 Giza, Egypt*

[5]*Solid State Physics Department, National Research Center, Dokki, Giza 12311, Egypt*

[6]*Chemistry Department, Faculty of Science, Suez Canal University, Ismailia, Egypt*

[7]*Univ. Lille, CNRS, Centrale Lille, ENSCL, Univ. Artois, UMR 8181 - UCCS - Unité de Catalyse et Chimie du Solide, F-59000 Lille, France*

[8]*Univ. Lille, CNRS, Centrale Lille, ISEN, Univ. Valenciennes, UMR 8520 - IEMN, F-59000 Lille, France*

**The Corresponding Author:*
E-mail: maaismail@yahoo.com
Tel: +966560480239

1. Physical characterizations

An Analytical Scanning Electron Microscope (SEM) JEOL JSM 6390 LA, with an EDS attachment (JEOL EDS EX-54175JMU) was used to examine the morphology and composition of the synthesized catalysts.

XPS measurements were performed with an ESCALAB 220 XL spectrometer from Vacuum Generators featuring a monochromatic Al Kα X-ray source (1486.6 eV) and a spherical energy analyzer operated in the CAE (constant analyzer energy) mode (CAE=100 eV for survey spectra and CAE = 40 eV for high-resolution spectra), using the electromagnetic lens mode. The detection angle of the photoelectrons is 30°, as referenced to the sample surface. After subtraction of the Shirley-type background, the core-level spectra were decomposed into their components with mixed Gaussian-Lorentzian (30:70) shape lines using the CasaXPS software. Quantification calculations were performed using sensitivity factors supplied by PHI. Gold was used to calibrate the XPS binding-energy scale.[1]

Structural characterization of the films was undertaken by X-ray diffraction using a Rigaku SMARTLAB multi-purpose 6-axis diffractometer (9 kW rotating anode) in grazing incidence configuration. Indeed, X-ray diffraction measurements of "thin" (10-1000 nm) films using classical θ-θ scanning modes generally produces a week signal from the film and an intense signal from the substrate. One of the ways to avoid such intense signal from the substrate and get stronger signal from the film itself is to perform a 2θ scan with a fixed grazing angle of incidence, known as GIXRD. The fixed angle was adjusted for each sample to give the maximum signal of the film compared to the substrate.

High-resolution TEM (HRTEM) images of Au NPs in solution (unsupported Au NPs) were recorded with a JEOL JEM-3100 operating at 220 kV. The UV-Vis spectra were recorded with Perkin Elmer, Lambda 25, in the 300-800 nm range, at a resolution of 1 nm. 30 mL of the separated gold nanoparticles were concentrated by centrifugation at 13,000 rpm for 25 min. The supernatant was

removed and settled nanoparticles were suspended in 5 mL deionized water with ultrasonication, then used for HRTEM characterization and loading glassy carbon electrode (R=3 mm).

2. SCE stability

The concern about the SCE stability originates from its instability in alkaline electrolytes, as diffusion of OH^- into the reference electrode might change the SCE to Hg/HgO with time, although this would take a very long time. To avoid such problem, the reference electrode was immersed in a Luggin capillary (Princeton Applied Research) filled with 2 M potassium nitrate (KNO_3, Sigma Aldrich) solution. This capillary acts as the salt bridge to minimize the junction potentials, and prevent contamination of the test solution (the alkaline environment) with Cl^- in the SCE. The Luggin capillary can also limit significantly diffusion of OH^- into the reference electrode, thus hindering the change of the SCE to Hg/HgO (although this would take a very long time). This in turn will maintain the potential of the SCE stable throughout the run.[2]

To ensure SCE (immersed in 2 M KNO_3 filled Luggin capillary) potential stability, we tested it (as a working electrode) against Hg/HgO as the reference electrode, and monitored the open-circuit potential (E_{oc}) for 3h, see Figure S1.

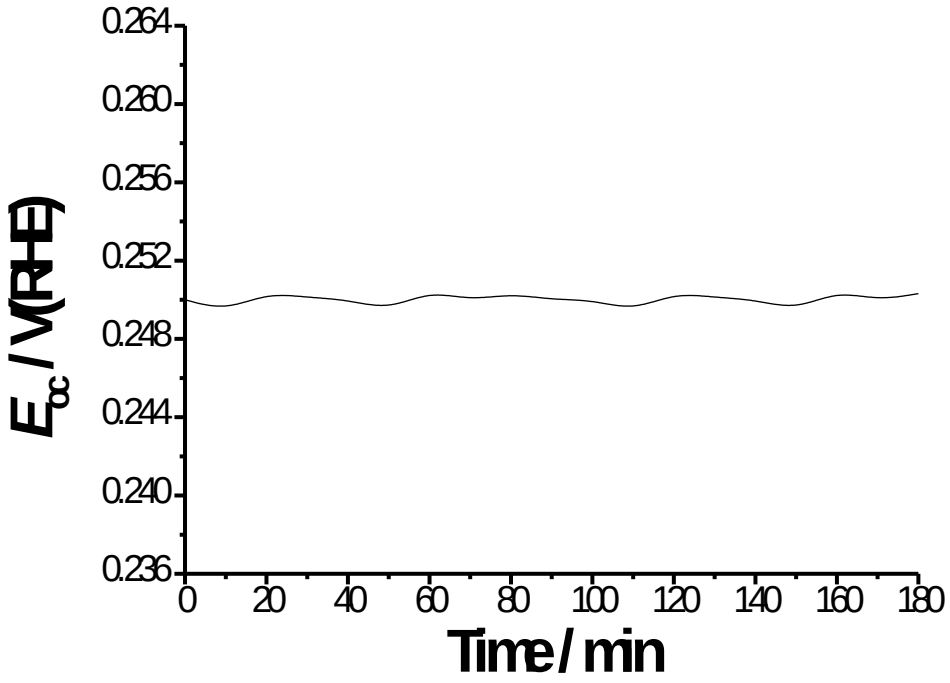

Figure S1: Testing SCE potential stability *vs.* Hg/HgO reference electrode in 0.1 M KOH solution at 25 ^{o}C.

It follows from Figure S1 that the E_{oc} of SCE retains its stability around 0.25 V *vs.* RHE over 3 hours with < 1 mV fluctuation, while each of our experiments was typically finished within 20 min at the latest. Therefore, our electrochemical set up here was very reliable for electrochemical measurements.

3. Conversion of the working electrode's potential from the SCE scale to the RHE scale

In this work, the potentials were measured with respect to SCE (E_{SCE} or $E_{electrode}$) and are reported *vs* reversible hydrogen electrode (RHE), E_{RHE}. Conversion to RHE was done using the relation:[3]

$$E_{RHE} = E_{SCE} - E^{o}_{H2/2H+} + 0.244 \quad (1)$$

where $E^{o}_{H2/2H+}$ is the reversible hydrogen potential, given by Nernst equation ($E^{o}_{H2/2H+}$ = -0.059 pH); a pH value of ~ 13 was measured for the test solution (0.1 M KOH). The number +0.244 in Eq. (1)

denotes the standard potential (in Volts) of the used SCE {Cl^- (4M) | $Hg_2Cl_{2(s)}$ | Hg(l) | Pt @ 25 ^oC). For instance, for $E_{electrode}$ = -2 V(SCE), E_{HER} = (-2) – (-0.059 × 13) + 0.244 = -0.989 V(RHE).

4. Faradaic efficiency measurements

The amount of H_2 produced for each catalyst during a controlled potential electrolysis was measured by gas chromatography (GC). Experiments were conducted in a custom-made airtight electrolysis cell containing 0.1 M KOH solution by holding the electrode at -0.8 V vs RHE for 1 h. Gas chromatography was conducted on an Agilent 7890A gas chromatograph, with a pneumatically operated automatic gas sampling valve to monitor the evolved H_2 gas. The electrolysis cell was connected to the gas chromatography system via bespoke airtight glass-to-metal adapters and copper tubing with an internal diameter of 1/8 in. The oven temperature was set to 45 °C, and the carrier gas was Ar with a flow rate of approximately 3 mL min^{-1}.

5. Particle size distribution of the supported Au NPs of catalysts 3-6.

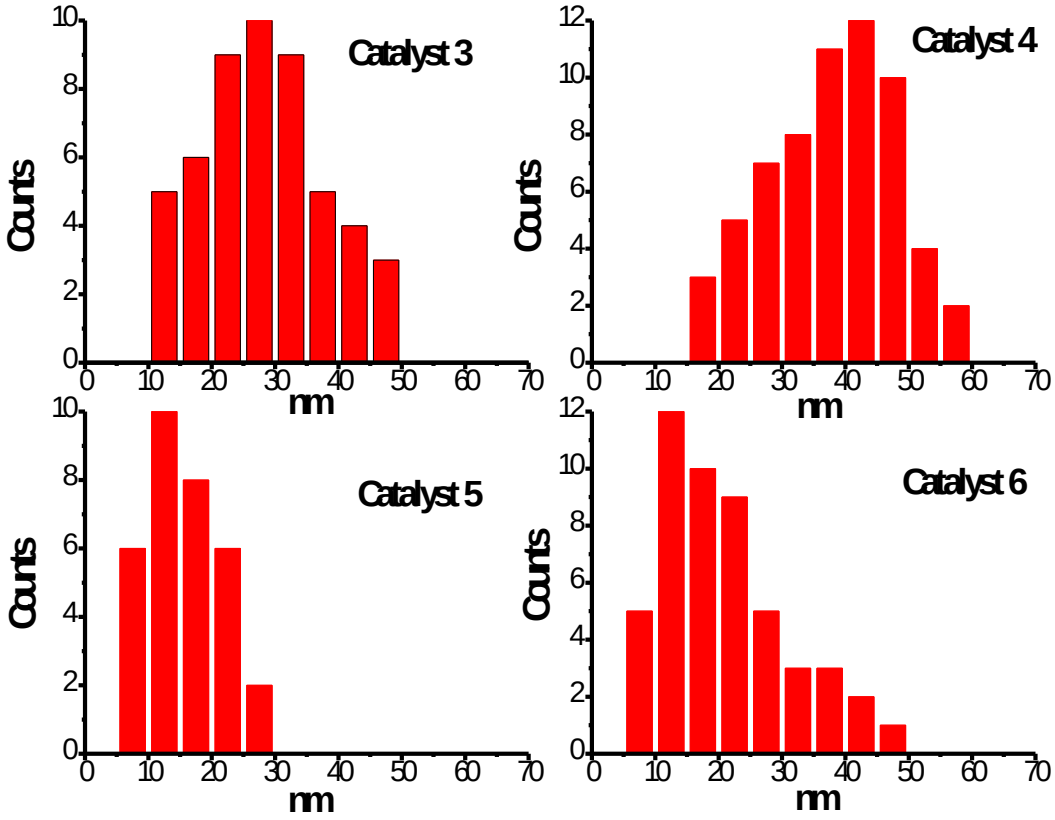

Figure S2: Particle size distribution of the supported Au NPs of catalysts 3-6.

6. SEM/EDX of catalysts 1 and 2.

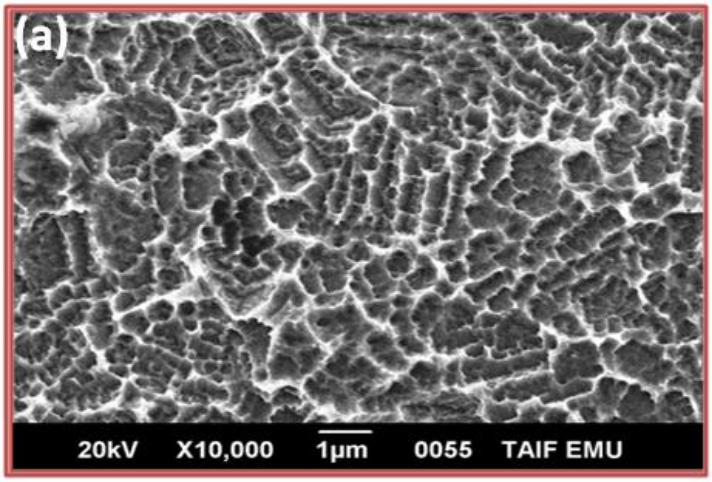

Element	KeV	Mass%
Ti	4.508	94.36
O	0.525	4.21
S	2.307	1.43

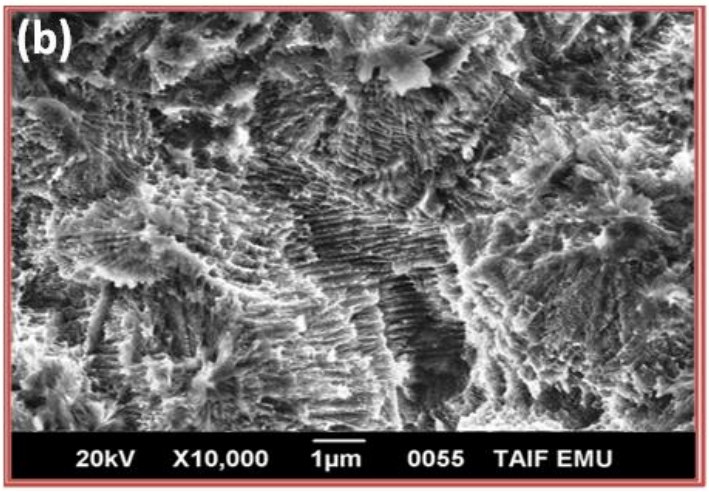

Element	KeV	Mass%
Ti	4.508	92.25
N	0.392	3.62
O	0.525	2.88
S	2.307	1.25

Figure S3: SEM/EDX of (a) catalyst 1 and (b) catalyst 2.

7. SEM/EDX and elemental mapping of catalyst 4.

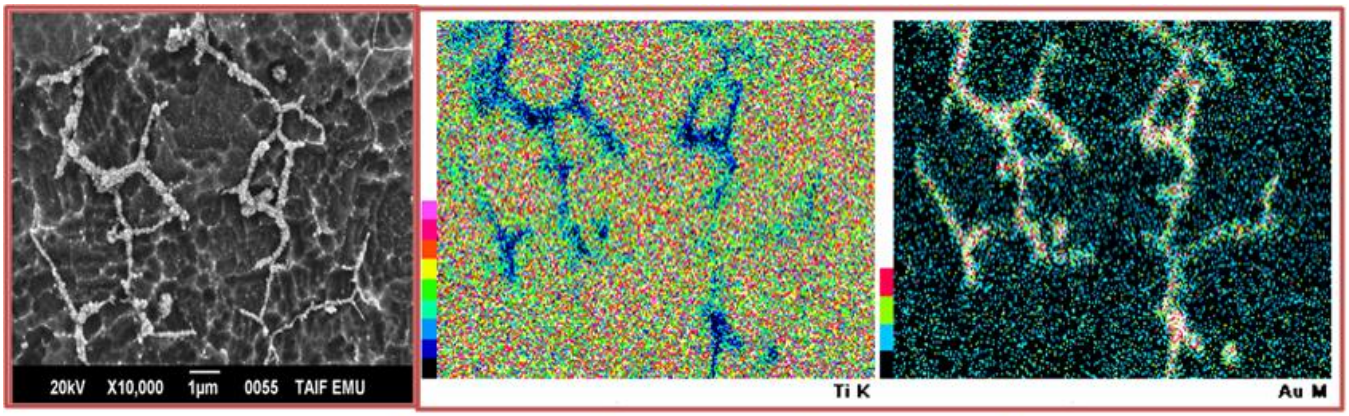

Element	keV	Mass%
Ti	4.508	80.04
Au	2.121	11.28
N	0.392	0.1
O	0.525	8.4
S	2.307	0.08

Figure S4: SEM/EDX and elemental mapping of catalyst 4.

Figure S4 presents the element mapping and SEM/EDX of catalyst 6. It could be clearly seen from elemental mapping that Au and O, in addition to minor contributions from N and S, truly existed in the sample. The contribution of O is increased from 2.88% in case of catalyst 2 (a supported Au NPs-free catalyst) to 8.4 (i.e., almost tripled) on the surface of catalyst 4 (an etched Ti-supported Au NPs catalyst). It seems that supported Au NPs catalyze the reduction of water for the HER and in the same time enhance substrate oxidation (passivation). The passivation influence of metallic nanoparticles supported on Ti was reported previously in our laboratory.[4,5] The presence of the supported Au NPs covering some parts of the substrate surface, besides their catalytic impact on substrate passivation, may account for the minor contribution of N and S as compared with their contributions on catalyst 2.

8. Values of roughness factor estimated from impedance measurements

Table S1 – Mean values of the roughness factor (R_f) obtained from EIS technique for the studied catalysts. EIS measurements were conducted in 0.1 M KOH solutions at cathodic potentials -0.3, -0.5, and -0.7 V *vs* RHE at 25 ^{o}C. The theoretical (calculated) value of Q equals 20 S^n (ω^{-1} cm^{-2}) for smooth polycrystalline Ti electrode.[6,7]

Catalyst	E / V (RHE)	$Q_{measured}$ = $(Q_1 + Q_2)^*$	R_f = $Q_{measured}$ / $Q_{calculated}$
As-polished (unmodified) Ti	-0.3	29.4	1.47
	-0.5	36.8	1.84
	-0.7	50.6	2.53
Catalyst 1	-0.3	1866.3	93.3
	-0.5	2252	112.6
	-0.7	2565	128.3
Catalyst 2	-0.3	2279	114
	-0.5	2649	132.5
	-0.7	2982	149
Catalyst 3	-0.3	6650	333
	-0.5	7332	367
	-0.7	8055	403
Catalyst 4	-0.3	8497	425
	-0.5	9331	467
	-0.7	10022	501
Catalyst 5	-0.3	11564	578
	-0.5	14503	725
	-0.7	16761	838
Catalyst 6 (the best)	-0.3	16681	834
	-0.5	19843	992
	-0.7	23056	1153
Catalyst 6**	-0.3	20279	1014
	-0.5	23588	1179
	-0.7	28507	1425
Pt/C	-0.3	20071	1004
	-0.5	23126	1156
	-0.7	28250	1413
TiH_2-free nanoporous Ti***	-0.3	2923	146.2
	-0.5	3225	161.3
	-0.7	3592	179.6

**values of Q_1 and Q_2 were taken from Table 2 in the main manuscript*

***catalyst 6 after 10,000 of repetitive cycling in 0.1 M KOH aqueous solutions at 25 ^{o}C. The cathodic cyclic polarization curves were swept between E_{corr} and -0.75 V vs. RHE at a scan rate of 50 mV s^{-1}.*

*** *prepared via immersing Ti in 10 M lactic acid solution containing 1.0 M NH_4F at room temperature for 60 min (see morphologies in Figure S6)*

9. Complex-plane impedance plots measured for the studied catalysts at -0.5 and -0.7 V *vs.* RHE

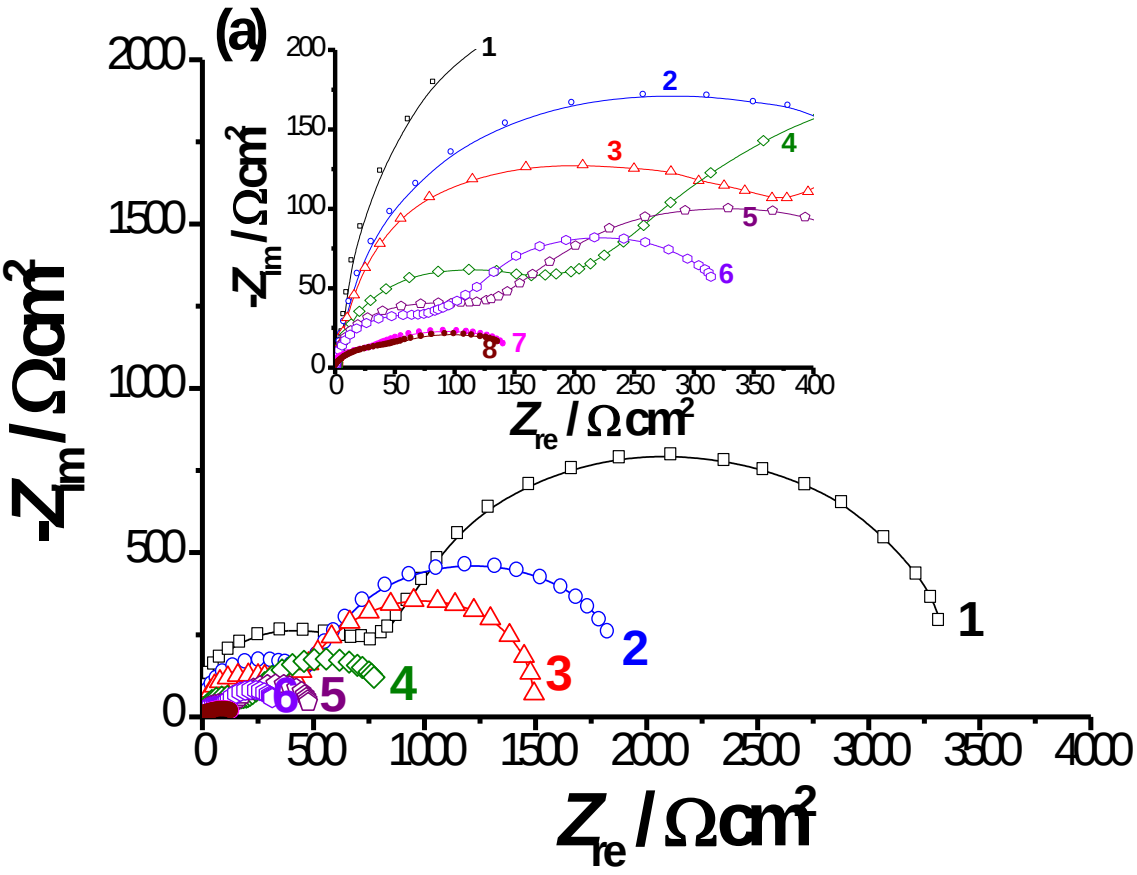

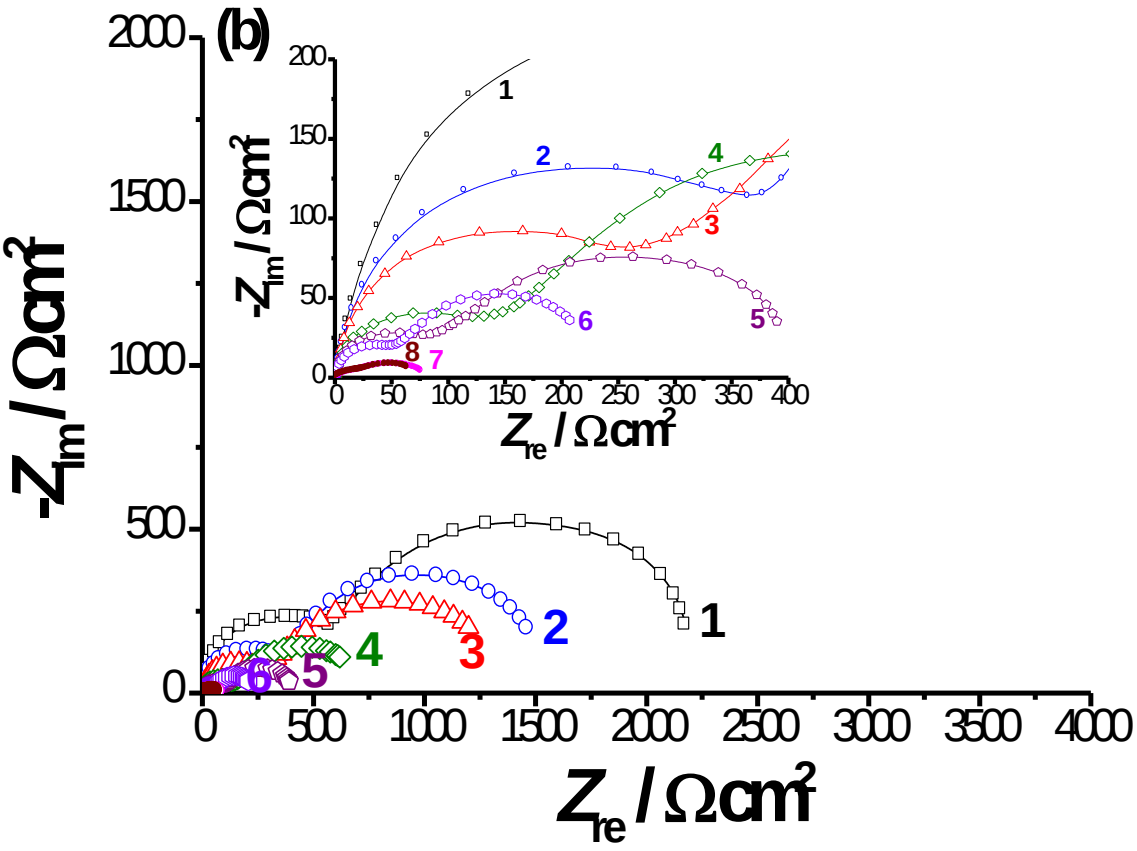

Figure S5: Complex-plane impedance plots recorded for the studied catalysts in comparison with bare (unmodified) Ti and Pt/C catalysts. Measurements were conducted in 0.1 M KOH solutions at (a) -0.5 V vs. RHE and (b) -0.7 V vs. RHE. (1) bare Ti; (2) catalyst 1; (3) catalyst 2; (4) catalyst 3; (5) catalyst 4; (6) catalyst 5; (7) catalyst 6; (8) Pt/C.

10. The equivalent circuit used to model and analyze the experimental impedance data

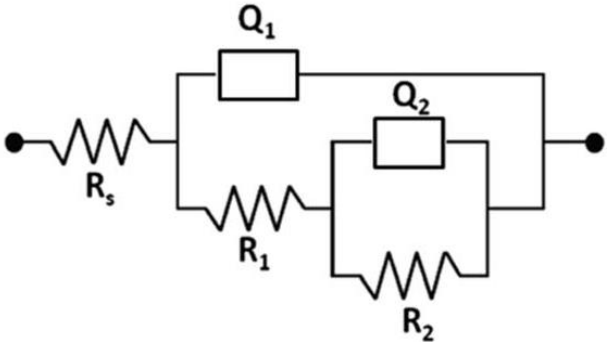

Figure S6: The equivalent circuit used to fit the experimental impedance data.

11. Low angle (2^o) XRD and SEM examinations for a TiH_2-free nanoporous Ti catalyst.

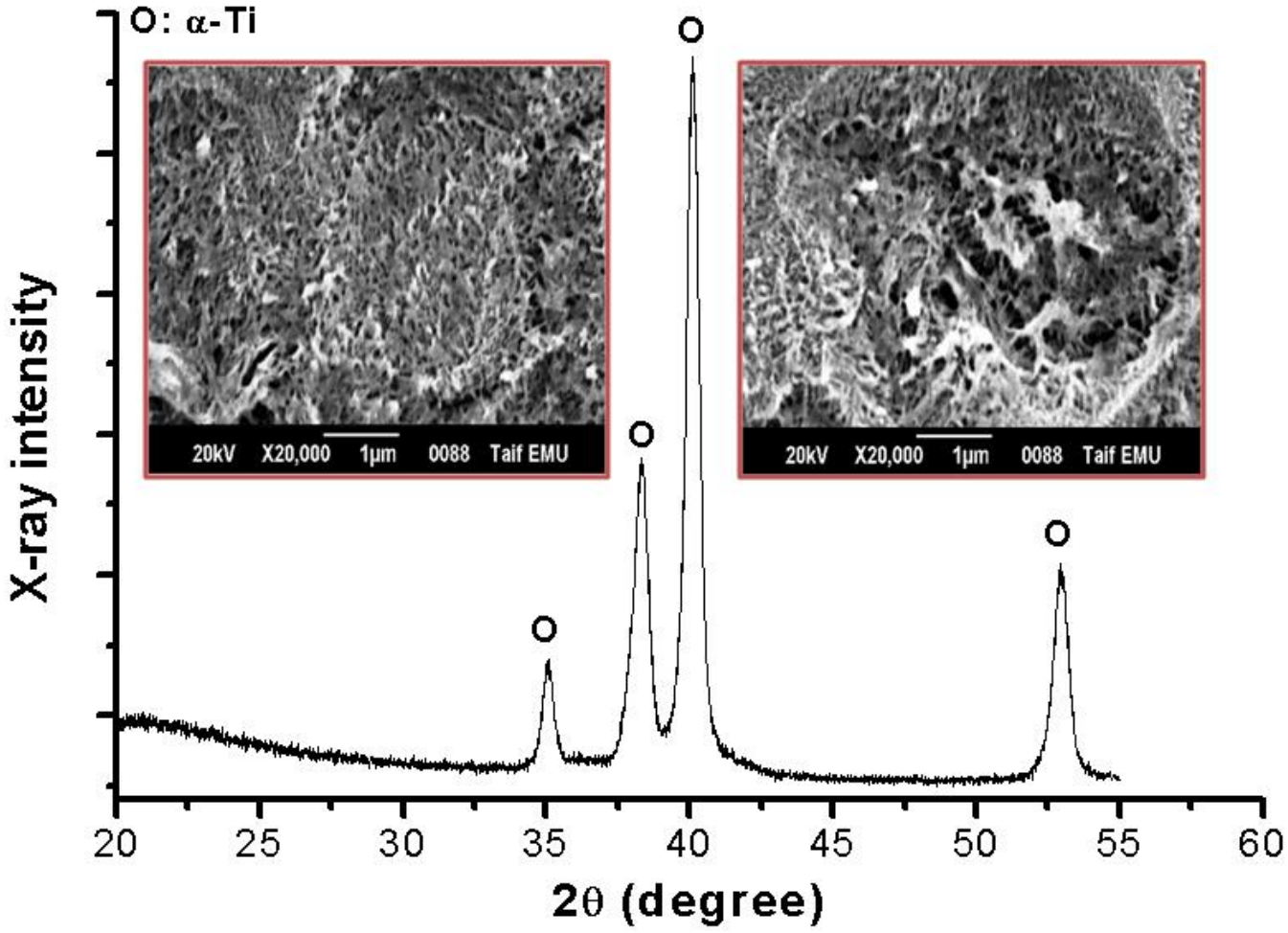

Figure S7: SEM images recorded at two different places of the same sample and its low angle (2^o) XRD diffraction pattern recorded for Ti after 60 min of chemical etching in 10 M lactic acid solution containing 1.0 M NH_4F at room temperature.

XRD revealed diffraction peaks due to α-Ti, located at 2θ of 35.0°, 38.4°, 40.2°, and 52.9° diffracted from the (100), (002), (101), and (102) planes (Reference code: 01-089-4893, crystal system: Hexagonal structure, space group P63/mmc). Peaks for any TiH_x phase not detected.

12. Cathodic polarization curve and Tafel analysis for a TiH_2-free nanoporous Ti catalyst.

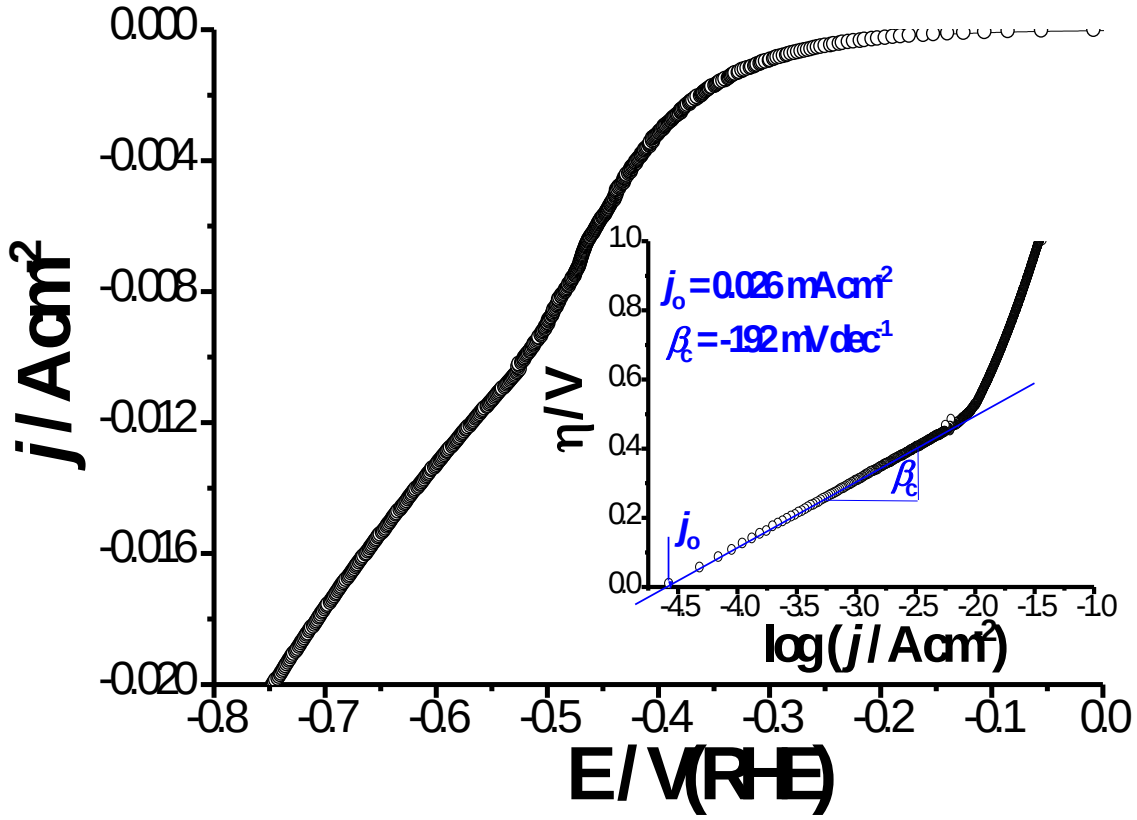

Figure S8: Cathodic polarization curve and its corresponding Tafel plot (inset), recorded for the TiH_2-free nanoporous Ti catalyst (its morphology is shown in the inset of Figure S6) in 0.1 M KOH solution at a scan rate of 5 mV s^{-1} at room temperature.

References

1. Seah, M. P. Post-1989 calibration energies for X-ray photoelectron spectrometers and the 1990 Josephson constant. *Surf. Interface Anal.* **1989**, *14*, 488.

2. Wang, H,; Lee, H.-W.; Deng, Y.; Lu, Z.; Hsu, P.-C.; Liu, Y.; Lin, D.; Cui, Y. Bifunctional Non-Noble Metal Oxide Nanoparticle Electrocatalysts Through Lithium-induced Conversion for Overall Water Splitting. *Nat. Commun.* **2015**, *6*, 7261-7268.

3. Cha, H. G.; Song, J.; Kim, H. S.; Shin, W.; Yoon, K. B.; Kang, Y. S. Facile Preparation of Fe_2O_3 Thin Film with Photoelectrochemical Properties. *Chem. Commun.* **2011**, *47*, 2441-2443.

4. Amin, M. A.; Fadlallah, S. A.; Alosaimi, G. S. Activation of Titanium for Synthesis of Supported and Unsupported Metallic Nanoparticles. *J. Electrochem. Soc.* **2014**, *161*, D672-D680.

5. Amin, M. A.; Fadlallah, S. A.; Alosaimi, G. S. In situ aqueous synthesis of silver nanoparticles supported on titanium as active electrocatalyst for the hydrogen evolution reaction. *Int. J. Hydrogen Energy* **2014**, *39*, 19519-19540.

6. Losiewicz, B.; Budniok, A.; Rowinski, E.; Lagiewka, E.; Lasia, A. The structure, morphology and electrochemical impedance study of the hydrogen evolution reaction on the modified nickel electrodes. *Int. J. Hydrogen Energy* **2004**, *29*, 145-147.

7. González-Buch, C.; Herraiz-Cardona, I.; Ortega, E. M.; García-Antón, J.; Pérez-Herranz, V. Development of Ni-Mo, Ni-W and Ni-Co Macroporous Materials for Hydrogen Evolution Reaction. *Chem. Eng. Trans.* **2013**, *32*, 865-870.